DFT+U accurate for strain effect and overall properties of perovskite oxide ferroelectrics and polaron

Watanabe, Yukio
Open Design Lab, Kyushu University

出版情報：Journal of Applied Physics. 135 (22), pp.224103-1-224103-16, 2024-06-14. AIP Publishing
バージョン：

Journal of Applied Physics

RESEARCH ARTICLE | JUNE 14 2024

DFT + *U* accurate for strain effect and overall properties of perovskite oxide ferroelectrics and polaron

Yukio Watanabe

J. Appl. Phys. 135, 224103 (2024)
https://doi.org/10.1063/5.0213487

Journal of Applied Physics ARTICLE pubs.aip.org/aip/jap

DFT + *U* accurate for strain effect and overall properties of perovskite oxide ferroelectrics and polaron

Cite as: J. Appl. Phys. **135**, 224103 (2024); doi: 10.1063/5.0213487
Submitted: 10 April 2024 · Accepted: 26 May 2024 ·
Published Online: 14 June 2024

Yukio Watanabe[1,2,a)]

AFFILIATIONS

[1]Open Design Lab, Kyushu University, Fukuoka, Japan
[2]Graduate School of Engineering, University of Hyogo, Himeji, Japan

[a)]**Author to whom correspondence should be addressed:** watanabe@phys.kyushu-u.ac.jp

ABSTRACT

We find that the unit cell volume (V), which affects many properties, decreases too rapidly with strain when calculated with standard density functional theories (DFTs) such as local density approximation (LDA). We find that this demerit is moderated with the use of the Hubbard potential U for local electron correlation (DFT + U). However, the introduction of U to standard DFTs, e.g., LDA and Perdew–Burke–Ernzerhof functional (PBE) optimized for solids (PBEsol), leads to the excessive underestimation of the spontaneous polarization (P_S) and frequently extinguishes P_S. Therefore, we attempt to improve the overall accuracy of DFTs for ferroelectrics by using U in several DFT methods including PBE that overestimates P_S and lattice constants. We demonstrate that PBE with U (PBE + U) is in excellent agreement with the experimental properties of $BaTiO_3$ and $SrTiO_3$, with improvements in the estimates of lattice constants, P_S, the phonon frequency, the antiferrodistortive angle of 105 K-phase $SrTiO_3$, the bandgap, the strain dependence of V, and hole polarons. When the lattice parameters and P_S moderately agree with the experimental data, PBE + U with a single U set can produce both electron and hole polarons. Hence, PBE + U can be a practical substitute of hybrid functionals for perovskite oxide ferroelectrics, except for the estimation of the bandgap. Furthermore, we propose an approach to construct a functional accurately depicting the incipient ferroelectric state of $SrTiO_3$. Additionally, these results suggest that conventional DFT underestimates P_S under compressive in-plane strain and predicts the unrealistic deformation of ferroelectrics and that in-plane-strained lattices can mitigate the problems associated with U.

I. INTRODUCTION

Ferroelectrics (FEs) are key insulators employed in a wide range of applications,[1] with advancements in FE technology, such as the development of monolayer FEs[2] and the non-contact control of both electron (e^-) and hole (h^+) layers.[3] FEs have electrically reversible spontaneous polarization (P_S) and an anisotropic lattice without inversion symmetry.[1] For tetragonal FEs such as $BaTiO_3$ (BTO) at room temperature (RT), this anisotropy is expressed as c/a (where c is the c lattice constant and a is the a lattice constant) and is correlated with P_S. Hence, the accurate estimation of the lattice parameters is the basis of the *ab initio* analysis of FEs. For FEs, the required accuracy is far stricter than for other materials [e.g., 0.5% for BTO and 0.1% for the incipient FE $SrTiO_3$ (STO),[4–6] surpassing the potential accuracy of standard density functional theories (DFTs) such as local density approximation (LDA) [local spin density approximation (LSDA)].[7] For this, an accurate e^- distribution is necessary because of the entanglement of e^- and ions.

For an accurate e^- distribution, *ab initio* theory is also expected to include electron correlation (e^- correlation) because it exists theoretically and in experiments appears as e^- localization (e.g., polarons). To date, *ab initio* theories have been improved by updating LDA to advanced exchange correlation (XC) functionals, including generalized gradient approximation (GGA), meta-GGA approximation, and hybrid functionals,[8–15] while LDA, GGA, and meta-GGA are DFTs. In GGA such as Perdew–Burke–Ernzerhof (PBE) functional,[8] the energies are expressed by the e^- density (n) and its derivative ($|\nabla n|$). Perdew *et al.*[8] explained that GGA expands and softens atomic bonds and tends to predict more

accurate total and atomization energies than LDA. According to Perdew *et al.*,[9] within a GGA framework, the accuracy of atomization and total energy is incompatible with that of the lattice constants and vice versa. In addition, PBE[8] has a stronger $|\nabla n|$ dependence and yields atomization and total energies that are more accurate than the PBE functional optimized for solids (PBEsol), which has a weaker $|\nabla n|$ dependence.[9]

Calculations using PBEsol have been shown to agree with the lattice constants of many solids and FE properties.[5,6,9] PBEsol is claimed to be accurate for "weakly varying valence-electron densities in densely packed solids" such as metals but is considered inaccurate for large values of $|\nabla n|$.[9] Because this trade-off between the atomization/total energy and lattice constants is present "within the framework of GGA,"[9] lower accuracy for the atomization and total energies, especially for non-metals, is expected for other GGA methods optimized for solids.[10]

The weaker $|\nabla n|$ dependence of PBEsol[9] leads to a lower sensitivity to the changes in $|\nabla n|$. This reduced sensitivity and the inaccuracy for large values of $|\nabla n|$[9] are expected to reduce the sensitivity of PBEsol to compressive strain (u_{ext}), which increases $|\nabla n|$. This lower sensitivity is also expected for LDA because LDA has no $|\nabla n|$ effect. In many situations, FEs are placed under mechanical stress or strain, including at domain boundaries (DBs) and at the interface with other materials. This strain has been known to change P_S and induce/extinguish the FE phase[16–25] at least since Devonshire's Ginzburg–Landau (GL) theory.[16,25–27] In particular, in tetragonal FEs, a giant increase in P_S by epitaxial strain is explicitly shown theoretically in 1994,[21,25] which is seen even in a starting GL equation without manipulations.[28,29] Furthermore, a 100% increase in the P_S and Curie temperature of a thin film compared to the bulk values was experimentally shown in 1997[19,20] much before it became widely known.[30] Accordingly, developing a theory that accurately predicts strain effects is important. In addition, the correct treatment of polarons[31–38] is required to understand electric field effects and FE domains.[2]

A representation of strain is the change in the unit cell volume (V), which reflects the average atomic interaction. In Fig. 1(a), V/V_0 (V_0: V at $u_{ext} = 0$) calculated using different *ab initio* methods are compared with experiments and a linear elastic theory (Poisson effect),[39] which is valid for a small $|u_{ext}|$. Figure 1(a) shows that V/V_0 calculated using the PBE functional stops to decrease at a small compressive in-plane strain (u_{ext}), while those calculated using PBEsol and LDA stop to decrease only at large values of $|u_{ext}|$. The PBE functional is, thus, more sensitive to u_{ext} than either PBEsol or LDA and produces the u_{ext}-dependence that is more consistent with a linear elastic theory at low $|u_{ext}|$ than PBEsol and LDA. We note that the Poisson ratio increases with strain, and when we consider this, the PBEsol and LDA results further deviate from the elastic theory. Similar results are obtained for STO (Sec. III C). In an experimental comparison using thin films,[40,41] defects and dislocations, which reduce or increase V, are unavoidable, especially at $u_{ext} < -0.01$. In the remainder of this paper, BTO is referring to the tetragonal (P4 mm) phase of BTO, unless otherwise mentioned.

In other words, PBEsol and LDA predict over-compressed lattices, and the arguments advanced by Perdew *et al.*[9] suggest that this also occurs with other GGA methods optimized for solids. This affects the accuracy of calculations of FE properties, with the

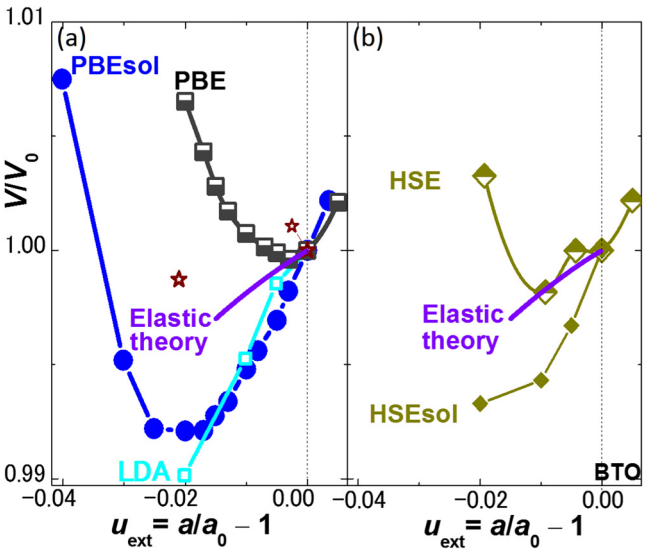

FIG. 1. Change in V of tetragonal BTO by in-plane strain ($u_{ext} \equiv a/a_0 - 1$) calculated using different XCs and linear elastic theory.[39] V_0 and a_0 are V and a at $u_{ext} = 0$ calculated using each XC, respectively. (a) PBE, PBEsol, and LDA. (b) HSE and HSEsol. Asterisks show the experimental data,[40,41] of which samples are considered to be sufficiently oxidized to reduce secondary phases and defects. The results with LDA and HSEsol are reprinted with permission from Y. Watanabe, J. Chem. Phys. **148**, 194702 (2018).[42] Copyright 2018 AIP Publishing.

underestimation of V resulting in the underestimation of P_S and the stability of the FE phase because P_S tends to increase with $c/a = V/a^3$ (Refs. 4, 5, and 42) and the stability of the FE phase increases with P_S (Refs. 6 and 42).

A difference similar to that in Fig. 1(a) is observed in the comparison of two hybrid functionals: Heyd–Scuseria–Ernzerhof (HSE) functional and the HSE functional for solids (HSEsol)[14,15] [Fig. 1(b)], where the DFT parts are PBE and PBEsol, respectively. Remarkably, the u_{ext}-dependence calculated using HSE and HSEsol agrees better with a linear elastic theory[39] than PBE and PBEsol [Fig. 1(b)], while HSE and HSEsol contain a local e^- correlation to circumvent the self-interaction of e^- intrinsic to DFTs.

The local e^- correlation can also be implemented in DFTs through Hubbard U. The use of Hubbard U to a meta-GGA method Tao-Perdew-Staroverov-Scuseria functional (TPSS)[11,43,44] improved the agreement with a linear elastic theory (Appendix B), while both TPSS and TPSS + U produce lattice and FE properties that agree with experimental data at $u_{ext} = 0$.[42] These results suggest that the implementation of local e^- correlation improves the accuracy in strain effects.

Local e^- correlation has been reported to be essential when determining the electronic and lattice properties of insulators and is a key factor for phase stability.[31–38,45–47] This also suggests that a DFT method with appropriate XC would agree with experimental data when the correlation is included. Accordingly, the agreement of DFT methods, which do not consider the correlation, with experimental data may be non-natural, while any disagreement between the two may indicate the possibility that the DFT method can be improved by including the correlation. In contrast, we find

that the inclusion of the correlation in DFT methods optimized for solids weakens the optimization; for example, PBEsol + U and LDA + U radically decrease the P_S of BTO as shown in Sec. III A. Hence, we seek to improve the accuracy of *ab initio* calculations of BTO and STO by including local e^- correlation (U) in DFT methods that are not optimized for solids. We find that DFT methods that overestimate the lattice constants and P_S (e.g., the PBE functional) are useful for DFT + U, while LDA underestimates the lattice constants and P_S[8,42] and is, thus, unsuitable.

In terms of the use of Hubbard U, the valence and the conduction bands of ABO_3 oxides generally exhibit O- and B-site characteristics, respectively, where A is a non-transition metal element such as Ca, Sr, Ba, K, Pb, and Bi and B is a transition metal element. Because the FE in ABO_3 is mainly due to B and O atoms,[42] we consider here BO_3, where B is at the center of symmetry.

The available implementation of U in the DFT is formulated in a spherically invariant manner.[43,44] In BO_3, the anisotropy of the orbits of the B residing at the center of symmetry is essential for FE, while three O's are present at peripherals. Thus, the impact of U on the inversion asymmetry, which is fundamental to the FE phase, is considered to be much severer at B than at O. Furthermore, U on B decreases n in anisotropic orbits, while U on O does not much (Appendix C). Hence, we expect that U on B (d-orbits) intrinsically reduces/destroys P_S; Sec. III A shows that DFT + U using standard values of U for Ti[48–52] destroys the FE phase [PBEsol + U + V (Ref. 52) is reported to retain FE]. Hence, we use U on O_{2p}[42,53,54] and a small U on Ti_{3d}.

An ideal *ab initio* theory would agree with all of the reliable experimental properties near 0 K when quantum fluctuation is negligible. We believe that this comprehensive agreement is the best criterion for the reliability of a particular calculation. We, thus, show that the PBE + U results agree with the major experimental properties of BTO and STO, including the lattice parameters, P_S, the strain dependence of V and P_S, phonon frequency,[17,19,40,41,55–64] and the formation of h^+ (and e^-) polarons, while also improving the estimation of the bandgap (Eg) and antiferrodistortive (AFD) distortion angle (φ).[65,66] When limited to FE phases ($P_S \neq 0$), these achievements of DFT + U have not been previously reported. In addition, the computational cost of PBE + U is orders of magnitude lower than that of hybrid functionals, which is valuable for large-scale calculations.

We study RT-phase BTO (tetragonal, P4 mm, C^1_{4v}) and RT-phase (cubic-tetragonal, Pm3m–P4 mm, O^1_h-C^1_{4v}), 105 K-phase (I4/mcm, D^{18}_{4h}), and 105 K FE-phase STO with P_S // c (I4 cm, C^{10}_{4v}). The RT-phase BTO is present down to 4 K in epitaxial films.[22] Theoretically, STO is in a FE phase at 0 K in the absence of quantum fluctuation,[6] which explains the appearance of the FE phase induced by negligible stress or impurities in experiments.[17,18]

II. METHODOLOGY

We define the renormalized local e^- correlation term U_{eff} as $U_{eff} \equiv U - J$, where U is the coulomb term and J is the exchange term. DFT methods that employ U_{eff} on Ti_{3d} and O_{2p} orbits are reported to predict e^- and h^+ polarons, respectively.[49–53] It is reported that the values of U and J are obtained *ab initio*,[48,67] such as through linear response theory, and U_{eff} for Ti_{3d} (U_{eff}(Ti)) and U_{eff} for O_{2p} [U_{eff}(O)] are approximately 4.5 and 9 eV, respectively.[51,52] It is also reported that standard values for U_{eff}(Ti) and U_{eff}(O) are determined to reproduce the experimental values for the Mott–Hubbard bandgap,[43,44,68,69] polaron,[49,50,53,54] or experimental Eg[70] and are typically 4–10 eV and 8–10 eV, respectively. Additionally, it is reported that the value of U_{eff}(Ti) is determined to reproduce the phase stability[45] and reaction energy,[71] which are typically 5 and 2–3 eV, respectively. We find that the DFT methods with these U_{eff} values do not achieve the accuracy required for the lattice parameters and FE properties of BTO and STO. We believe that this is partly due to the restriction posed by spherically invariant formulation[43,44] and, thus, self-consistent U values[48,52,67] are also approximations. We find that the use of different atomic potentials [projector augmented wave (PAW) potentials[72]] in PBE, PBEsol, LDA, TPSS, and SCAN does not resolve this disagreement.

Lattice constants reflect ion–ion, e^-–ion, and e^-–e^- interactions, while the internal atomic coordinates contribute much less to the total energy than do the lattice constants.[6,73] Hence, we choose U_{eff} to reproduce the experimental lattice constants under stress-free conditions, while $J = 0$ for O (i.e., $U_{eff} = U$) and J for Ti is a standard value, e.g., 0.5 eV.[49–51]

Logically, the criterion of accuracy for DFT methods with FEs is the agreement with experiments near 0 K, because native *ab initio* calculations predict the properties at 0 K under no quantum fluctuation. However, the conventional criterion is in agreement with experiments at RT, but such an agreement can be due to error compensations and, hence, may mean some insufficiencies of the DFT. Furthermore, the effects of temperature and quantum fluctuation are trivial compared with those of mechanical strain[19–24,40,41] and an unscreened depolarization field.[28,74] For example, epitaxial strain retains a BTO RT phase down to 4 K in experiments.[22] Hence, in many cases, including the calculation of RT properties, it is logically and practically preferable for the criterion of accuracy for DFT methods to be in agreement with experiments at 0 K. Because these experiments on FEs are rare, we proposed a process for deducing 0 K properties from experiments above 0 K[42] and used these 0 K properties as the accuracy criterion (Fig. 2 and Table I). However, we also show that by choosing U, PBE + U can reproduce the experimental properties at RT and under quantum fluctuations (Sec. III).

In the present study, all calculations are performed using PAW potentials[72] as implemented in VASP,[75–77] with a plane wave energy cutoff of 650 eV. In the geometry relaxation and Berry phase calculation of P_S,[78] the Monkhorst–Pack[79] mesh for Brillouin-zone integration is $8 \times 8 \times 8$ for the RT phases (unit cell size: 4 Å × 4 Å × 4 Å) and $8 \times 8 \times 6$ for the STO 105 K phase (unit cell size: 5.5 Å × 5.5 Å × 8 Å), respectively; the results are almost the same for other mesh sizes, e.g., $6 \times 6 \times 6$ – $13 \times 13 \times 13$ for the RT phases or $6 \times 6 \times 4$ for the 105 K phase, being consistent with Wahl *et al.*[5] P_S is also estimated using a semiempirical formula.[80] After relaxation, the calculated forces are at least lower than 0.5 meV/Å. The screening parameter (μ) in HSE06 and HSEsol is a default value (0.2 $Å^{-1}$).[5] The results of stress-free BTO and stress-free cubic and 105 K-paraelectric STO calculated using LDA, PBEsol, PBE, and HSE are used to test the reliability of the calculations and agree with the results presented by Wahl *et al.*,[5] including the zone-

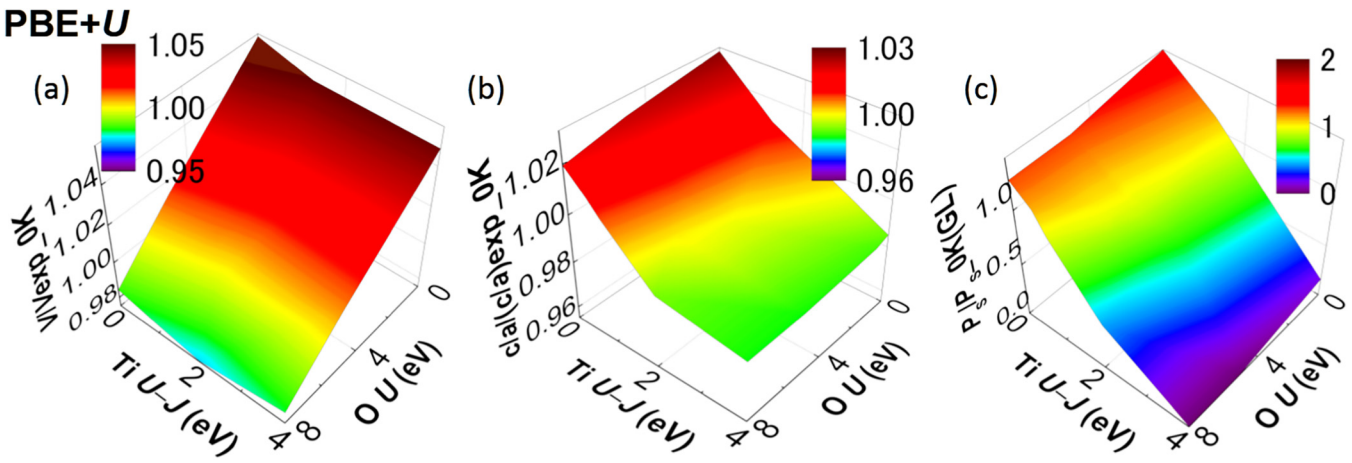

FIG. 2. *U*-dependence of (a) V/V_{exp}, (b) $c/a/(c/a)_{exp}$, and (c) P_S/P_S^{exp} of a BTO calculated using PBE + *U*. V_{exp}, $(c/a)_{exp}$, and P_S^{exp} are experimental estimates at 0 K.[42] Experimental values correspond to *yellow* in color scale.

center phonon frequencies. For the 105 K FE phase of STO, the HSE calculations[6] agree with experimental results.[17,59,65,66] In the calculation of polarons for excess e^- or h^+, the Makov–Payne scheme[81] implemented in VASP and graphics-processing-unit acceleration[82,83] are used. Ion positions and charge and spin density (unpaired e^- density) are also visualized using VESTA.[84]

The default PAW potentials used in the present study are those recommended for metal oxides by the VASP manual: Ba_{SV} for Ba, Sr_{SV} for Sr, Ti_{SV} for Ti, and O_s for oxygen (energy cutoff: 283 eV). VASP provides three PAW potentials for oxygen. In some cases, such as for a large U_{eff}(Ti), the standard PAW potential for oxygen (energy cutoff: 400 eV) is used (denoted as O_{st}). Another PAW potential for oxygen (O_h, energy cutoff: 700 eV) offers little advantage when it is used with Ba_{SV}, Sr_{SV}, and Ti_{SV} for BTO and STO.

III. RESULTS

A. Determining *U*

Figures 2 and 3 present the *U*-dependence of *V*, *c*/*a*, and P_S of BTO and STO calculated using PBE + *U*, respectively, and compare them with experimental results or reliable theoretical values (Tables I and II).[55–59,85–88] Among examined DFT + *U*'s, only PBE + *U* achieves the agreements of all of *V*, *c*/*a*, and P_S with reliable values.

U_{eff}(O) reduces *V*, *c*/*a*, and P_S. U_{eff}(Ti) keeps *V* almost unchanged, decreases *c*/*a*, and drastically decreases P_S, which implies the incompatibility of U_{eff}(Ti) with the FE phase. U_{eff}(O) and U_{eff}(Ti) increase h^+ and e^- polaron binding energy, respectively. These trends and improvements in accuracy are also found in other DFT methods (Appendix A).

The use of O_{st} instead of O_s increases *V*, *c*/*a*, and P_S (Appendix A), which is useful for the use of a large U_{eff}. Additionally, PBEsol agrees with most experiments at $u_{ext} = 0$,[5,42] but PBEsol + *U* and LDA + *U* disagree with the experiments, except for using O_{st} with extremely small values of U_{eff}(O) (Tables I and II).

B. Comparison with experiments under no external stress

Table I, Fig. 2, and Appendix A show that the experimental *V*, *c*/*a*, and P_S (at 0 K) of RT-phase BTO are reproduced by PBE + *U*, while PBEsol + *U* O_{st}, LDA + *U* O_{st}, and SCAN + *U* failed. Table I lists the typical cases and shows that *Eg* is also improved by U_{eff}(O). The comparison of different DFT methods in Fig. 4 and Table I shows that the accuracy of PBE + *U* and TPSS + *U* O_{st} is comparable with or better than that of PBEsol. PBE + *U* can also reproduce the experimental properties at RT by choosing U_{eff}'s [e.g., U_{eff}(O) = 6 eV, U_{eff}(Ti) = 1.6 eV (Fig. 4)].

In Fig. 3 and Table II, the experimental *V* and *c*/*a* and the reliable theoretical P_S of RT-phase STO under no quantum fluctuation and no stress[6,58,59] are reproduced by PBE + *U* with U_{eff}(O) = 4–6 eV and U_{eff}(Ti) = 0–0.3 eV.

Below 105 K, STO is in the 105 K phase.[17] In Fig. 5, the calculations of 105 K-phase STO are compared with experimental values in a pseudo-cubic unit cell representation.[6] When comparing HSE, HSEsol, PBE, PBEsol, TPSS + *U*, and LDA, only HSE yields lattice parameters (including φ) that agree with the experimental values.[6,58,59,65,66] In Figs. 5(a) and 5(b), PBE + *U* with the aforementioned U_{eff}(O) and U_{eff}(Ti) noticeably improves the accuracy of these parameters and outperforms PBEsol.

The calculation with the HSE functional reveals that stress-free 105 K-phase STO at 0 K under no quantum fluctuation[87] is in an FE phase.[6] This agrees with the appearance of an FE phase with the application of negligible stress or negligible impurities[17,18] ($P_S = 1.5\,\mu C/cm^2$),[88] which suppresses quantum fluctuation. P_S predicted using the HSE functional is considered an upper bound,[6] whereas PBEsol and LDA fail to show FE phases.[6]

TABLE I. Typical results with DFT + *U* for BTO. The procedures for estimating *V*, *c*, and *c*/*a* at 0 K[42] are described in the caption of Fig. 4. The results by TSPP O_{st}, TSPP + *U* O_{st}, and PBEsol + *U* O_{st} agreed better with experimental data than those with O_s.

	U_{eff} O	U_{eff} Ti	*a* (Å)	*c* (Å)	*V* (Å^3)	*c*/*a*	P_S (μC/cm^2)	*Eg* (eV)
PBE	0	0	4.000	4.213	67.41	1.053	45.8	1.77
PBE + *U*	6	1	3.964	4.067	63.89	1.026	32.7	2.32
PBE + *U*	6	1.3	3.969	4.052	63.81	1.021	29.7	2.36
PBE + *U*	5.5	1.3	3.974	4.060	64.11	1.022	30.2	2.30
PBE + *U*	5	1.3	3.979	4.069	64.42	1.023	30.8	2.25
PBE + *U* O_{st}	8	0	3.983	4.186	66.41	1.051	44.6	1.93
PBE + *U* O_{st}	5	2	4.021	4.100	66.27	1.020	28.7	2.04
PBE + *U* O_{st}	5	3.2	4.039	4.046	66.00	1.002	9.5	2.12
PBE + *U* O_{st}	5	4.45	4.046	4.047	66.26	1.000	0.0	2.26
PBEsol[a]	0	0	3.971	4.059	64.01	1.022	32.5	1.75
PBEsol[b]	0	0	3.971	4.054	63.94	1.021	31.4	1.77
PBEsol O_{st}	0	0	3.962	4.096	64.29	1.034	40.5	
PBEsol + UO_{st}	0	0.3	3.971	4.054	63.93	1.021	31.91	
PBEsol + UO_{st}	0	1	3.979	4.034	63.88	1.014	25.8	1.87
HSE[a]	0	0	3.965	4.145	65.16	1.045	42.5	3.35
HSE[b]	0	0	3.965	4.145	65.16	1.045	42.5	2.92
HSEsol[a]	0	0	3.946	4.042	62.94	1.024	33.3	3.31
TPSS O_{st}[a]	0	0	3.989	4.070	64.76	1.020	31.8	1.79
TPSS + UO_{st}[a]	8	0	3.971	4.045	63.77	1.019	30.5	1.94
TPSS + UO_{st}	2	2	4.007	4.012	64.41	1.001	6.3	
SCAN	0	0	3.987	4.112	65.37	1.031	35.4	
SCAN + *U*	8	0	3.980	4.066	64.40	1.022	31.1	
SCAN + *U*	6	0.5	3.989	4.060	64.59	1.018	28.1	
LDA O_{st}[a]	0	0	3.941	3.990	61.97	1.012	26.1	1.75
LDA[b]	0	0	3.945	3.978	61.91	1.009	21.6	1.73
LDA + *U* O_{st}	6	0	3.928	3.965	61.17	1.010	22.6	
LDA + *U* O_{st}	0	6	3.987	3.986	63.36	1.000	0.4	
Exp. RT[c]			3.993	4.037	64.35	1.011	0.271[d]	3.27
Exp. (0 K)[a]			3.971	4.051	63.89	1.020	0.318 (0.321)	

[a]Reference 42.
[b]Reference 5.
[c]Reference 55.
[d]At 270 K.[56]

In the calculation with PBE + *U* with the same set of U_{eff}'s in Fig. 5, *V*, *c*/*a*, and φ of the FE 105 K phase are very close to *V*, *c*/*a*, and φ of the 105 K phase.

C. Strain dependence

Using the DFT + *U* methods with *U* values that yield the agreements with experimental properties at $u_{ext} = 0$, Figs. 6 and 7 reexamine u_{ext}-dependence. Similar results are obtained for the u_{ext}-dependence of *c*/*a*, as expected from that of *V* and $c/a = V/a^3$. The experimental data for $u_{ext} \leq -0.002$ are from epitaxial films, while defects in epitaxial film are considered to increase with $|u_{ext}|$, especially $|u_{ext}| > 0.01$.[30,89]

The results obtained with the PBE + *U* method are indicated by the reddish symbols. In Fig. 6, the dependences of V/V_0 and P_S of BTO given by the PBE + *U* method are closer at low $|u_{ext}|$ to a linear elastic theory and the experimental results than those given by the other DFT methods examined in Fig. 6 and Appendix B.

For STO, we show no plot of an elastic theory because the elastic constants of STO are sensitive to temperature and those near 0 K are absent.[90] The P_S of RT phase STO at $u_{ext} \approx 0$ is considered to be $>1.5\,\mu C/cm^2$ when quantum fluctuation is suppressed[17,88] because it is theoretically larger than P_S of 105 K phase.[6] The results calculated with PBE + *U*, PBEsol, and HSE are mutually similar (Fig. 7). In closer examinations of Fig. 7 and Appendix B, V/V_0 and P_S calculated with PBE + *U* agreed the

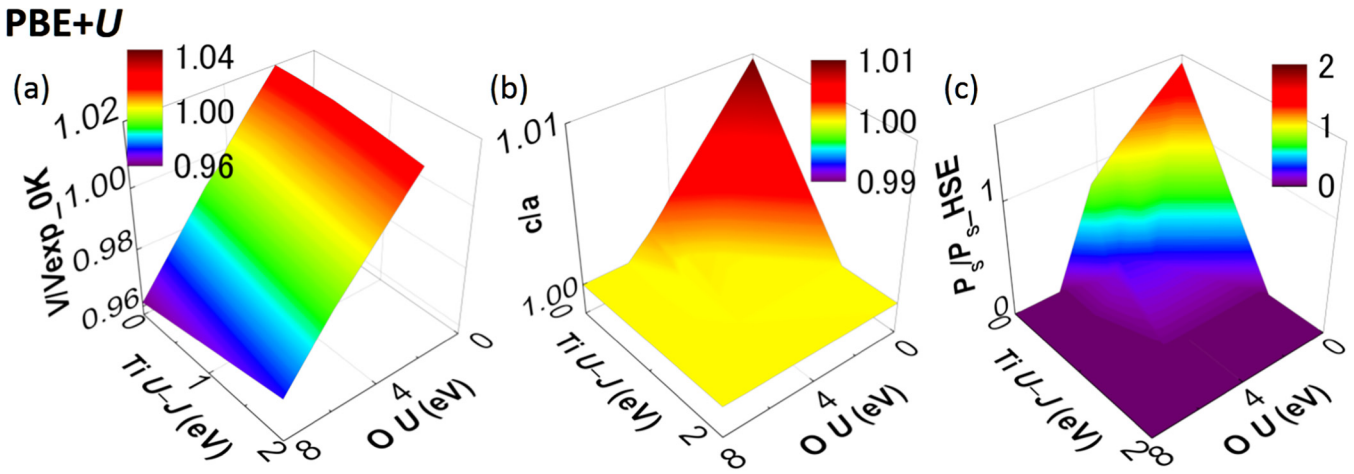

FIG. 3. *U*-dependence of (a) V/V_{exp}, (b) c/a, and (c) P_S/P_S^{HSE} of an RT phase STO calculated using different PBE + *U*. V_{exp} is an experimental *V*.[59] P_S^{HSE} is P_S given by HSE,[6] which was comparable with P_S given by PBEsol.[6] Experimental or HSE values correspond to *yellow* in color scale.

TABLE II. Typical results with DFT + U for STO. The differences between two HSE calculations[5,6] are due to the screening parameter (λ). a_{pc} and c_{pc} are *a* and *c* constants of the pseudocubic unit cell.

			RT phase (no AFD)			105 K phase (AFD)			105 K-FE phase (AFD + P_S)			
	U_{eff} O (eV)	U_{eff} Ti (eV)	a (Å)	c/a	P_S (μC/cm^2)	a_{pc} (Å)	c_{pc}/a_{pc}	φ (°)	a_{pc}	c_{pc}/a_{pc}	φ (°)	P_S (μC/cm^2)
PBE + *U*	4	0	3.900	1.003	15.1	3.897	1.003	3.71				
PBE + *U*	4.3	0	3.897	1.003	13.8	3.894	1.002	3.60	3.893	1.005	3.89	13.1
PBE + *U*	4.3	0.3	3.900	1.000	2.5	3.896	1.003	3.80	3.896	1.003	3.80	2.9
PBE + *U*	4.5	0.3	3.898	1.000	2.2	3.894	1.003	3.70	3.894	1.003	3.74	0.8
PBE + *U*	6	0	3.878	1.000	0.0	3.876	1.002	2.87				
PBE + *U*	6.7	4.45	3.899	1.000	0.0	3.890	1.005	5.39				
PBE + *U* O_{st}	8	0	3.909	1.008	23.2	3.908	1.003	4.17				
PBE			3.936	1.010	25.4	3.935	1.004	4.67				
PBE[b]						3.933	1.004	4.74				
HSE[a]			3.899	1.004	16.5	3.899	1.001	1.77	3.896	1.005	2.69	15.9
HSE[b]						3.900	1.001	2.63				
PBEsol[a]			3.897	1.001	7.3	3.888	1.005	5.25	3.888	1.005	5.25	0.0
PBEsol[b]						3.886	1.006	5.31				
LDA[a]			3.863	1.000	0.1	3.851	1.007	5.65	3.851	1.007	5.65	0.0
LDA[b]			3.863	1.000		3.847	1.008	6.05				
HSEsol[a]			3.872	1.000	0.2							
Exp.[c,d]			3.897	1.002		3.897	1.002	2.10				
Exp.[e,f]			3.896	1.001		3.896	1.001	>1.6				

[a]Reference 6.
[b]Reference 5.
[c]Reference 59.
[d]Reference 65.
[e]Reference 58.
[f]Reference 66.

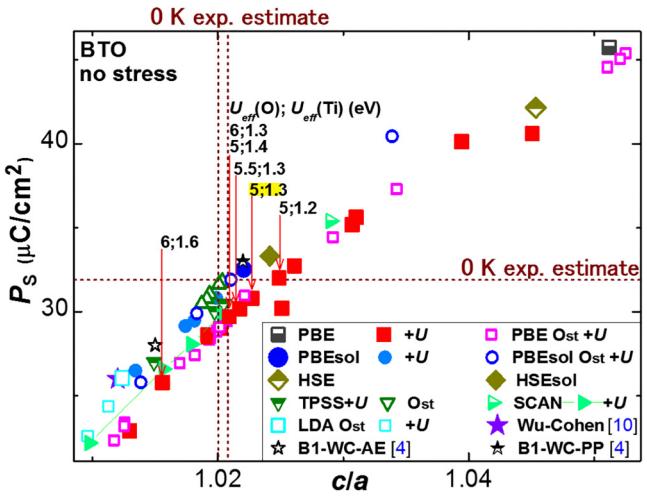

FIG. 4. P_S and c/a of stress-free BTO calculated using different XCs and Us. XCs without U are replots from Ref. 42. Dashed lines show the experimental values estimated at 0 K.[42] c/a is given by $c/(V/c)^{1/2}$, where c is estimated by a GL theory[42] and two values of V at 0 K are estimated by the extrapolations of three sets of experimental data.[55,85,86] P_S and c/a near RT are close to those of B1-WC-AE,[4] LDA O_{st}, PBEsol + U [U_{eff}(O) = 8 eV], and PBE + U [U(O) = 6 eV, U (Ti) = 1.6 eV].

best with those with HSE, while HSE produced the results agreeing the best with the experiments of STO.[6]

D. Phonon

The lack of experiments on strain effects in Fig. 7 is compensated by the experiments of the zone-center phonon frequencies, which reflect interatomic forces. The phonon frequencies of cubic BTO calculated with PBE + U and HSE ($\lambda = 0.3$ Å^{-1})[5] agree more closely with the experimental results than those calculated with the other *ab initio* methods in Fig. 8(a). This is consistent with the agreement of PBE + U results with an elastic theory in Fig. 6(a). The phonon frequencies of cubic STO calculated using PBE + U agree with the experimental results more closely than those calculated using the other *ab initio* methods in Fig. 9.

For tetragonal RT-phase BTO, the phonon frequencies using both PBE + U and PBEsol agree with the experimental data at $u_{ext} = 0$ [Fig. 8(b)], but PBE + U shows that the frequencies are more sensitive to u_{ext} than PBEsol.

E. Appropriate *U* and PBE + *U* for incipient FE

As shown in Figs. 2–9 and Tables I and II, the PBE + U method yields accurate lattice parameters, P_S, the u_{ext}-dependence, and phonon frequencies and improved *Eg*. Figures 6(b) and 7(b) show that the appropriate estimate of P_S under strain is much higher than the *ab initio* calculations predicted using LDA.

For the optimum PBE + U method, we list U_{eff}(O) = 5–6 eV and U_{eff}(Ti) = 0–1.5 eV for BTO and U_{eff}(O) = 4–6 eV and U_{eff}(Ti) = 0–0.3 eV for STO. The reason that these U_{eff} sets are not unique is that trade-offs exist and we include the U_{eff} sets that yield agreement with RT experiments of BTO (Tables I and II). With BTO, for example, U_{eff}(O) = 6 eV and U_{eff}(Ti) = 1.3 eV yield lattice constants that almost completely agree with GL estimates at 0 K, and P_S calculated using U_{eff}(O) = 6 eV and U_{eff}(Ti) = 1 eV or U_{eff}(O) = 5 eV and U_{eff}(Ti) = 1.3 eV agrees well with P_S at 0 K.

For both BTO and STO, the PBE + U method can also reproduce the experimental data at RT, by changing U_{eff}. For fine-tuning, the following results are useful (explained partly in Sec. III A). As seen in Figs. 2 and 3 for BTO and RT-phase STO, U_{eff}(O) reduces V, c/a, and P_S, while U_{eff}(Ti) almost does not change the V of BTO, reduces the V of RT-phase STO, and drastically reduces the c/a and P_S of BTO and RT-phase STO. As seen in Figs. 5(a) and 5(b) for 105 K-phase STO (paraelectric), U_{eff}(O) reduces V, c/a, and ϕ, while U_{eff}(Ti) increases V, c/a, and ϕ; the cause of these changes in c/a is considered due to that in ϕ.[6] In the case of 105 K-phase STO (P_S // c) [Fig. 5(c)], U_{eff}(O) reduces V, c/a, P_S, and ϕ, while U_{eff}(Ti) increases V and ϕ and decreases c/a and P_S.

As an application, we construct a functional for an incipient FE state of 105 K-phase STO. PBE + U with U_{eff}(O) = 6 eV and U_{eff}(Ti) = 0.145 eV yield c/a and ϕ that are consistent with the experimental ones (Fig. 5) and shows $P_S = 0$ for both 105 K-phase and FE 105 K-phase. We believe that this state is an incipient FE state, because PBE + U with U_{eff}(O) = 6 eV and U_{eff}(Ti) = 0, 0.1, 0.14, 0.143, 0.144, and ≥0.145 eV shows P_S = 1.6, 0.61, 0.009, 0.0003, 0.0002, and 0 μC/cm^2, respectively.

As discussed in Sec. I, Tables I and II and Figs. 2 and 3 show that the use of standard values for U_{eff}(Ti) is incompatible with FEs. Because the origin of this incompatibility is the spherically invariant formulation of U,[43,44] the same incompatibility should also occur with the use of standard values for U_{eff} for other transition metal elements such as Hf, Mn, Fe, and Nb. Indeed, the P_S of $BiFeO_3$ given by LDA + U ($U_{eff} = U = 5.3$ eV on Fe) is 30 μC/cm^2,[91] which is 35% of the correct P_S value.[92] Figures 6(a) and 7(a) also show that U_{eff}(Ti) softens the lattice of BTO and STO even more than PBEsol and LDA and yields incorrect lattice constants.

F. Electron localization: Polarons

The efficacy of U on e^- correlation is tested by observing polarons for excess h^+ or e^-. The minimum U_{eff} for polaron formation is about 3 eV, which is consistent with the study by Deskins and Dupuis;[50,53] no polarons are observed in the calculations using PBE and PBEsol. In Fig. 10, PBE + U with U_{eff}(O) = 6.7 eV and U_{eff}(Ti) = 4.45 eV yields both h^+ and e^- polarons, $P_S = 0$ and lattice constants that agree with experimental results for STO at RT.

As explained in Sec. III A– III D, overall agreement with experimental data including P_S and phonons is achieved using PBE + U with a range of U_{eff} values. Of these values, U_{eff}(O) = 5 eV and U_{eff}(Ti) = 1.3 eV for BTO and U_{eff}(O) = 4.3 eV and U_{eff}(Ti) = 0.3 eV for STO are used in Figs. 11(a) and 11(b).

In these cases, only h^+ polarons are observed in BTO and STO. These h^+ polarons are extended in the plane ⊥ P_S. The binding energy of the polarons increases with U_{eff}, and the binding energy of the polarons in STO [Fig. 11(b)] is slightly lower than 1 eV given by LDA + U.[54] On the other hand, PBE + U O_{st} [U_{eff}(O) = 5–8 eV and U_{eff}(Ti) = 3.2–3.3 eV] yields BTO properties

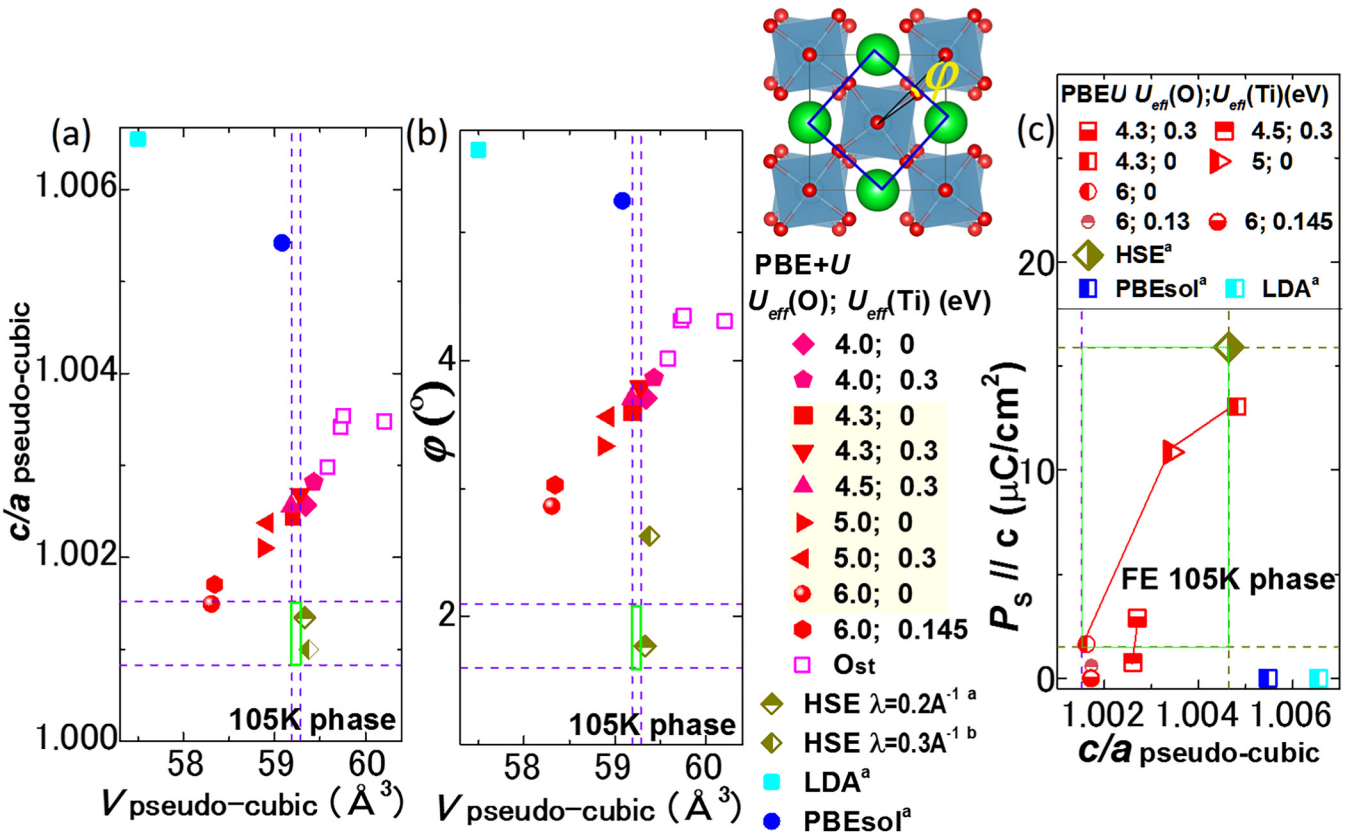

FIG. 5. 105 K-phase STO under no stress. (a) and (b) Paraelectric and (c) FE. $V_{\text{pseudo-cubic}}$ vs (a) $c/a_{\text{pseudo-cubic}}$ (V and c/a of pseudocubic unit cell) and (b) AFD angle φ. Dotted lines show the experimental values near 0 K (Refs. 58, 59, 65, and 66) and define an agreement criterion (green rectangle); in (c), the dotted lines show experimental $c/a_{\text{pseudo-cubic}}$ and P_S[88] of paraelectric STO near 0 K and P_S // c of given by HSE.[6] The blue square in the illustration shows the pseudo-cubic unit cell. [a]Ref. 6, [b]Ref. 5 (λ for HSE is 0.3 Å^{-1}). PBEsol and LDA overestimated φ and, hence, c/a.[6]

that modestly agree with experimental data, including P_S (Table I). PBE + U O_{st} with these U_{eff} values produces both h^+ polarons and marginally localized e^- polarons with a shallow binding energy [(Figs. 11(c) and 11(d)].

IV. SUMMARY

An ideal *ab initio* calculation is expected to agree with major reliable experimental properties near 0 K when quantum fluctuation is negligible, while the accurate estimation of the lattice parameters is the basis of *ab initio* calculations for FEs. This is almost satisfied when using appropriately chosen hybrid functionals[4,14,15,93,94] with parameters and atomic potentials (PAW potentials) selected.[4–6,42] However, hybrid functionals are computationally too heavy for large-scale calculations. Hence, a frequently used compromise is to use hybrid functionals for the ion positions given by DFT methods. This is an inconsistent method that is inappropriate because the ion positions given by DFT methods are different from those given by hybrid functionals (see Figs. 1–3 and 6) and electronic properties and ion positions are entangled (e.g., FE under depolarization field screened by excited e^-).[3,29,33] Hence, DFT methods that reach the performance level of hybrid functionals are desired.

For BTO and STO, GGA methods optimized for solids (e.g., PBEsol) overcome the inaccuracy of LDA[7] and are reported to perform well[5,6,42] except for 105 K-phase STOs, Eg, and polarons. However, we find improper u_{ext}-dependence of the V given by PBEsol and LDA, which is moderated in the calculations using PBE or the functionals that contain local e^- correlation (Fig. 1). This disagreement is a critical disadvantage because V is a fundamental output and affects many properties.[5,6,95] Because local e^- correlation exists in real insulators, we think that the agreement with experiments exhibited by DFT methods without the correlation may be non-natural, while the disagreement with experiments yielded by DFT methods without the correlation is natural. Meanwhile, we observe that the implementation of local e^- correlation to DFT (DFT + U) diminishes the FE properties. Thus, we expect that DFT + U based on DFT methods that overestimate FE properties[5,42] has the potential to achieve overall agreement with

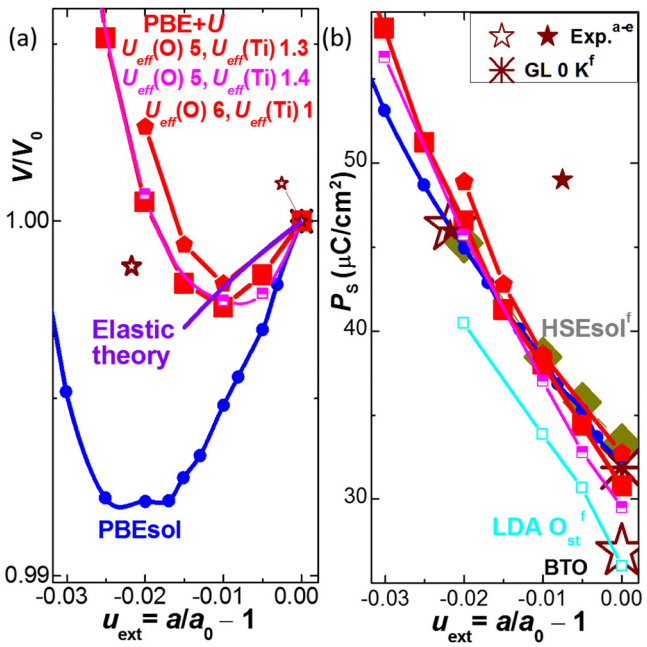

FIG. 6. In-plane strain dependence of (a) V and (b) P_S of tetragonal BTO (V_0 and a_0 are V and a at $u_{ext} = 0$, respectively, and calculated using each XC). For the two asterisks near $V/V_0 = 1$ in (a) and Fig. 1(a), V_0 and a_0 are V and a of a thick BTO film, in which strain is relaxed. References for [a–e] are 19, 30, 40, 41, and 55. The reference for [(f)] is 42.

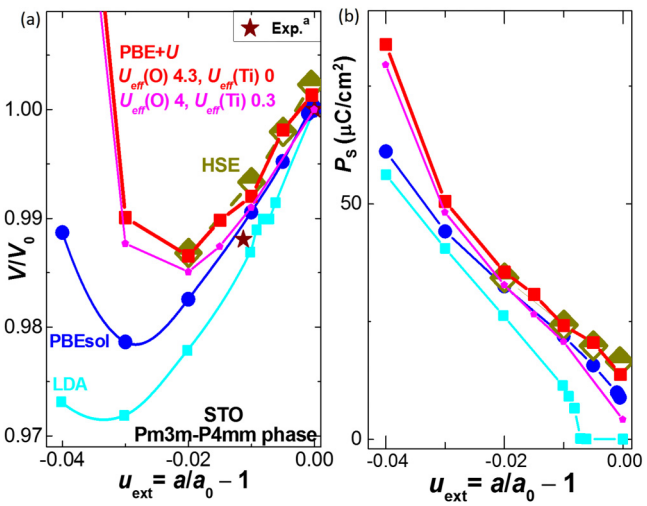

FIG. 7. In-plane strain dependence of (a) V and (b) P_S of RT-phase (Pm3m–P4mm) STO. The definition of V_0 and a_0 is given in Fig. 6. [a] is calculated from the experimental c in Ref. 89. In experiments, STO has $P_S \parallel c$ for $u_{ext} \lesssim -0.001$.[6,17] P_S by HSE, PBEsol, and LDA are from Ref. 6.

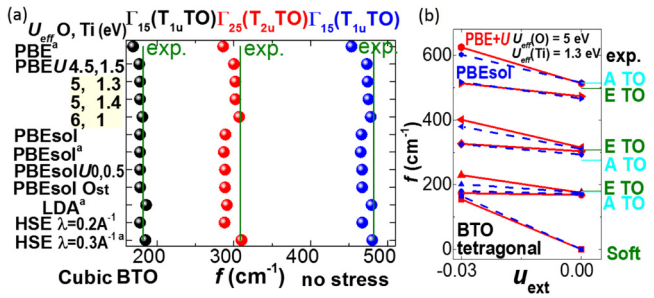

FIG. 8. (a) Zone-center phonon frequencies of cubic BTO. (b) u_{ext}-dependence of zone-center phonon frequencies of tetragonal BTO [PBE + U: U_{eff}(O) = 5 eV, U_{eff}(Ti) = 1.3 eV]. Experimental phonon frequencies (cm^{-1}) shown by green or light-blue lines ($u_{ext} = 0$) are 182, 308, and 482 for cubic BTO[60] and 178, 180, 276, 308, and 498, 515 for tetragonal BTO.[61] [a]Ref. 5.

experiments. This expectation is tested in the present study through the analysis of RT-phase (tetragonal) BTO, RT-phase STO (cubic-tetragonal), and 105 K-phase (I4/mcm) STO.

As discussed in Sec. I, the Hubbard U is formulated in a spherically invariant manner; thus, the standard or self-consistently derived value of U in the B atom in ABO_3 destroys the FE phase, as shown in Tables I and II and Figs. 2 and 3. Because of this and other justifications, we choose U_{eff} so as to yield the experimental lattice parameters at $u_{ext} = 0$ at 0 K. Of the DFT + U methods, PBE + U with U_{eff} chosen

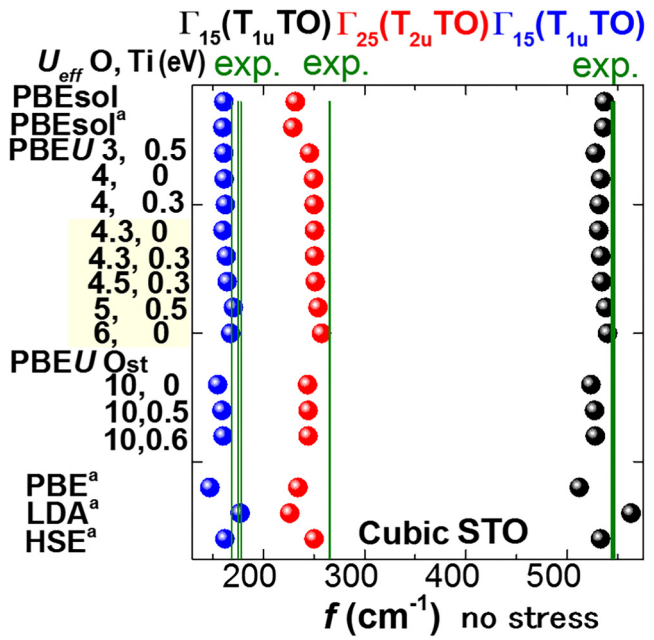

FIG. 9. (a) Zone-center phonon frequencies of cubic STO ($u_{ext} = 0$). Experimental phonon frequencies (cm^{-1}) shown green lines are 169 (175, 178), 265 (266, 266), and 545 (547, 544).[62–64] [a]Ref. 5.

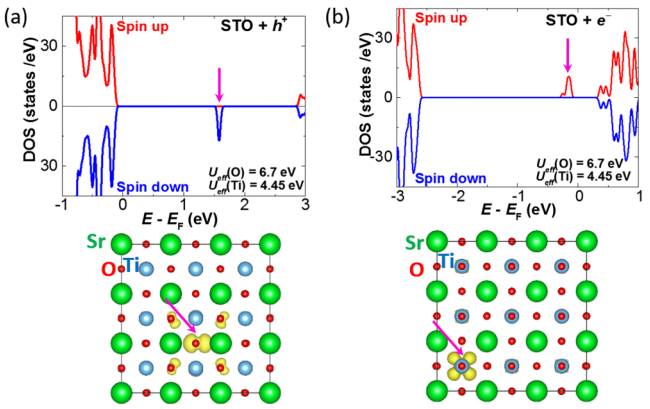

FIG. 10. Polaron for (a) an excess h^+ and (b) an excess e^- in STO, as shown by an isolated state in DOS and a localized unpaired e^- density (yellow shades). The central location of a polaron is at O (a) and Ti (b). Lattice distortions exist but invisible in (a) and (b).

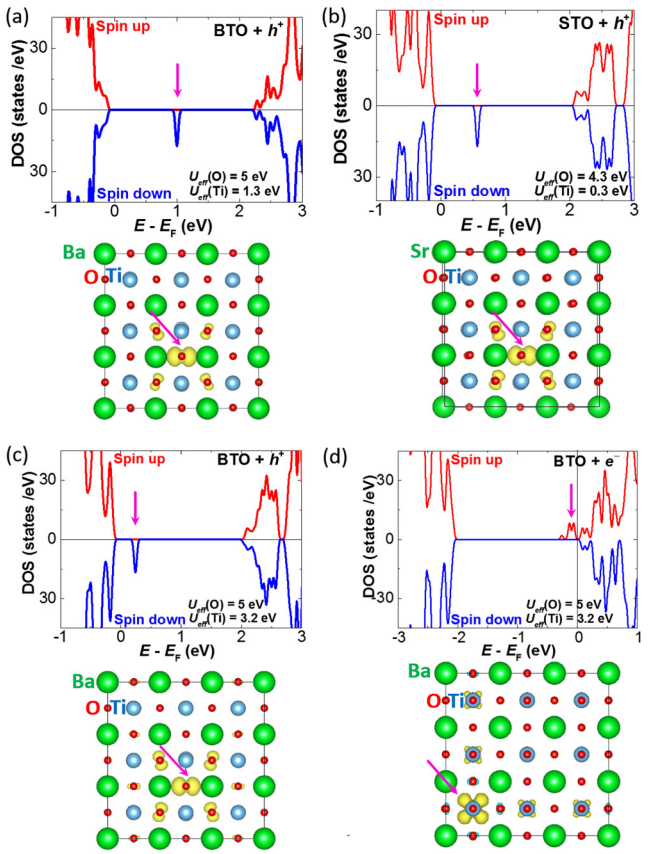

FIG. 11. h^+ polaron in (a) BTO and (b) STO for U_{eff} by which PBE + U excellently reproduces basic experimental properties. (c) h^+ and (d) e^- polaron in BTO shown with a single set of U_{eff} [U_{eff}(O): 5 eV, U_{eff}(Ti): 3.2 eV, O_{st}]. The results are shown in the same manner as Fig. 10.

in this manner reproduces experimental lattice constants, P_S, the u_{ext}-dependence of V, and phonon frequencies, noticeably improves the estimates of AFD φ (with which P_S changes critically [6]), and Eg, and shows h^+ polarons, similar to properly selected hybrid functionals. These values for U_{eff} are listed in Sec. III E, and the origin of the destruction of the FE phase is discussed in Appendix C. When we are satisfied with the modest agreement of the lattice parameters and P_S, PBE + U O_{st} with a single U_{eff} set is used to show both e^- and h^+ polarons (Sec. III F). Because of the effect of U on B and, especially, O atoms (Appendix C), PBE + U is expected to be also useful for other ABO_3 oxide FEs.

As mentioned above, PBE shows the moderate u_{ext}-dependence in the V and the overestimation of FE properties, which is more favorable for the implementation of U than PBEsol does. Because PBEsol is obtained by changing the gradient expansion coefficients μ and β of PBE,[9] adjusting μ and β is conjectured to further improve the accuracy of PBE + U.

Figures 6(b) and 7(b) show that the appropriate estimate of P_S under strain is considered to be much higher than that calculated with conventional DFT methods such as LDA and PBEsol, if a sample remains defect-free. Figures 1, 6, and 7 also indicate the possibility that conventional DFT methods predict unrealistic deformation that yields improper polarization configurations in FE domains. Additionally, Figs. 6 and 7 suggest that, by using an in-plane-strained lattice, PBE + U with standard values of U_{eff} can exhibit both an accurate P_S and e^-/h^+ polarons.

ACKNOWLEDGMENTS

This work was supported by Murata Science Foundation and KAKENHI under Grant No. JP19K21853. The discussions with P. Blöchel of TU Clausthal, K. Dayal of Carnegie Melon U., T. Yamada at Kyushu U., and N. Pertsev of Ioffe are greatly acknowledged.

AUTHOR DECLARATIONS

Conflict of Interest

The author has no conflicts to disclose.

Author Contributions

Yukio Watanabe: Conceptualization (equal); Data curation (equal); Formal analysis (equal); Funding acquisition (equal); Investigation (equal); Methodology (equal); Project administration (equal); Resources (equal); Validation (equal); Visualization (equal); Writing – original draft (equal); Writing – review & editing (equal).

DATA AVAILABILITY

The data that support the findings of this study are available from the corresponding author upon reasonable request.

APPENDIX A: *V*, *c*/*a*, AND P_S FOR OTHER DFT + *U*'s

Figures 12 and 13 present the *U*-dependence of *V*, *c*/*a*, and P_S of BTO and STO calculated using DFT + *U*'s of which accuracy is improved by the implementation of *U*.

APPENDIX B: ADDITIONAL RESULTS OF STRAIN DEPENDENCE

The u_{ext}-dependence of *V* and P_S of tetragonal BTO and RT-phase STO, which are not shown in Figs. 6 and 7, are displayed in Figs. 14 and 15. Either the *V*, *c*/*a*, ϕ, P_S at $u_{ext} = 0$, or the u_{ext}-dependence of *V* or P_S given by the *ab initio* methods using the parameters listed in Figs. 14 and 15 is inconsistent with experimental results or elastic theory, except for HSE and TPSS + *U* O_{st}.

APPENDIX C: ORIGIN OF EFFECTS OF *U*

We discuss the origin of the effects of *U*. Atomization and FE-phase energy are the basic outputs of *ab initio* calculations. BTO contains three O atoms and a Ti atom, and the effect of U_{eff}(O) in these energies is tripled. Hence, Fig. 16(a) shows that the effect of U_{eff} (O) on atomization energy is similar to that of U_{eff}(Ti); U_{eff} (O) and U_{eff}(Ti) reduce atomization energy similarly. Figure 16(a) shows that the atomization energy by PBEsol is larger than that by PBE and PBE + *U*. These results are consistent with the increase in the

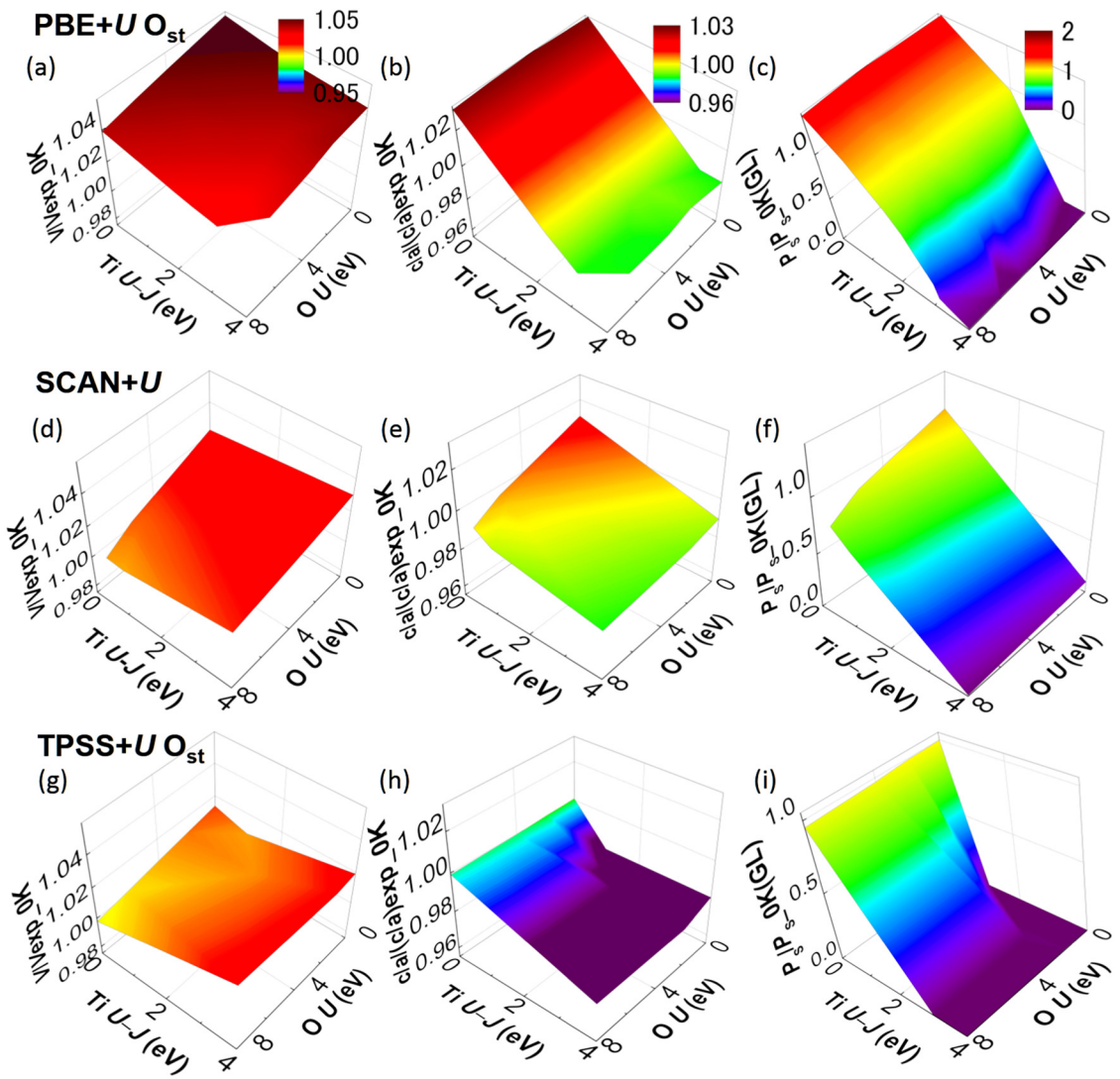

FIG. 12. *U*-dependence of a BTO by DFT + *U* other than PBE + *U* O_s (Fig. 2): (a) and (d) (g) V/V_{exp}, (b) and (e) (h) $c/a/(c/a)_{exp}$, and (c) and (f) (i) P_S/P_S^{exp}. (a)–(c) PBE + *U* O_{st}, (d)–(f) SCAN + *U*, (d)–(f) TPSS + *U*. In color scale, *yellow* corresponds to experimental values. V_{exp}, $(c/a)_{exp}$, and P_S^{exp} are experimental estimates at 0 K.[42]

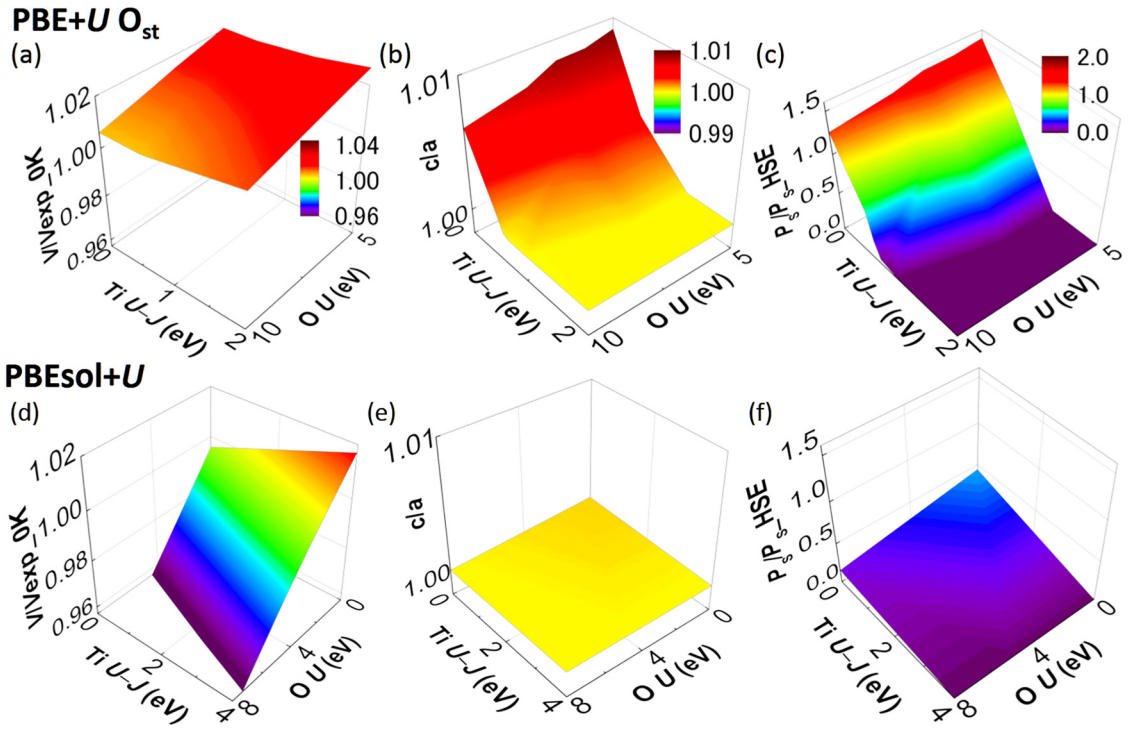

FIG. 13. *U*-dependence of RT phase STO by DFT + *U* other than PBE + *U* O_s (Fig. 3): (a) and (d) V/V_{exp}, (b) and (e) *c*/*a*, and (c) and (f) P_S/P_S^{HSE}. (a)–(c) PBE + *U* O_{st}, (d)–(f) PBEsol + *U*. Experimental or HSE values correspond to *yellow* in color scale. V_{exp} is an experimental *V*.[59] P_S^{HSE} is P_S given by HSE.[6]

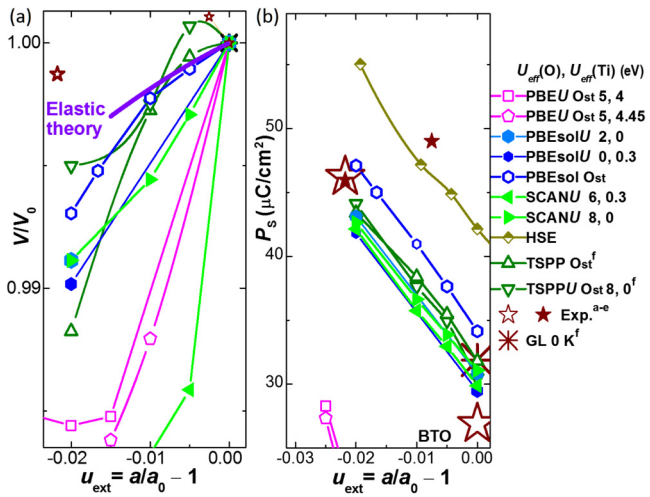

FIG. 14. u_{ext}-dependence of (a) *V* and (b) P_S of tetragonal BTO (supplementary to Fig. 6) (V_0 and a_0 are calculated using each XC). For the two asterisks near $V/V_0 = 1$ in Figs. 1(a) and 6(a), V_0 and a_0 are *V* and *a* of a thick BTO film, in which strain is relaxed. References for [a-e] are 19, 30, 40, 41, and 56. The reference for [f] is 42.

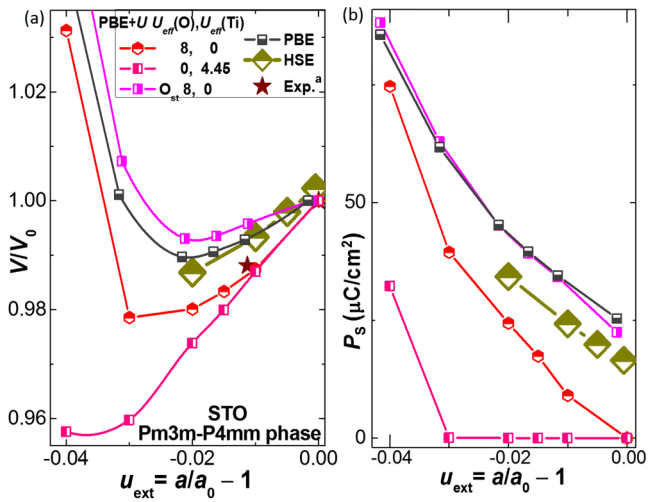

FIG. 15. u_{ext}-dependence of (a) *V* and (b) P_S of RT-phase (Pm3m–P4mm) STO (supplementary to Fig. 7). The definition of V_0 and a_0 are given in Fig. 6. [a]Calculated from the experimental *c* in Ref. 89. In experiments, STO has $P_S \parallel c$ for $u_{ext} \leq -0.001$.[6,17] P_S by HSE is from Ref. 6.

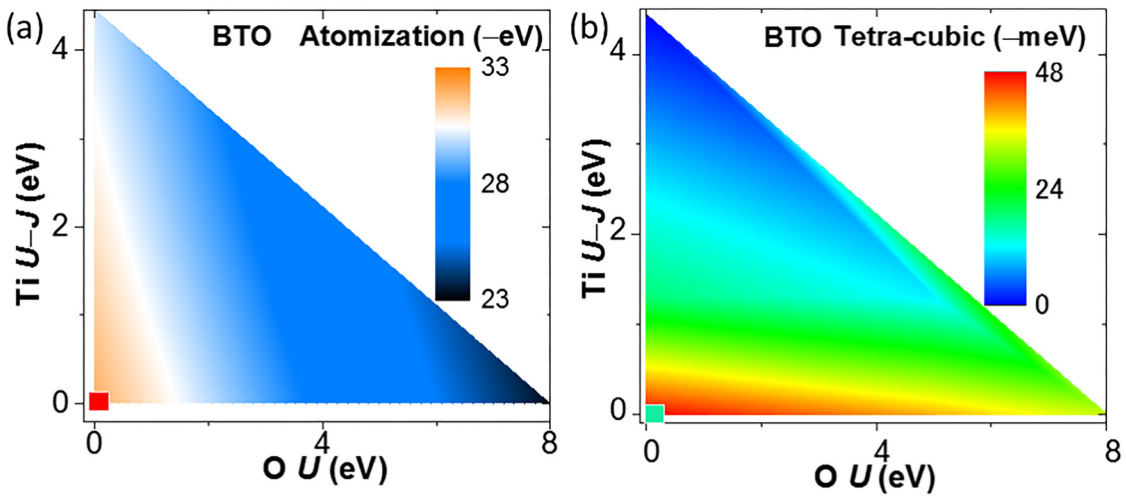

FIG. 16. (a) Atomization energy and (b) FE-phase energy (energy difference between tetragonal and paraelectric phase) of BTO given by PBE + *U*. The color (red, green) of small squares at the origin represent the energies given by PBEsol.

e^-e^- repulsion energy by *U* and the decrease in the interatomic distance by PBEsol. Contrastingly, U_{eff}(Ti) decreased FE-phase energy much more rapidly than U_{eff}(O) [Fig. 16(b)], which explains the rapid decrease of by P_S and *c*/*a* by U_{eff}(Ti) in Fig. 2. In Fig. 16(b), the FE-phase energy by PBEsol is clearly lower than that by PBE, which explains the more rapid decrease of P_S and *c*/*a* by *U* in PBEsol than that by *U* in PBE (Fig. 2).

Figure 17 examines these effects of U_{eff}(Ti) on FE-phase energy and P_S, using e^- distributions in a Ti atom. The e^- densities in Fig. 17 contain the densities of 3*p* e^-, 4*s* e^-, and 3*d* e^-. The unpaired e^- densities in Fig. 17 are due to the 3*d* e^-s that contribute to the chemical bonding with O atoms, and, hence, the effect of U_{eff}(Ti) on the bonding with O atoms is more visible than the e^-

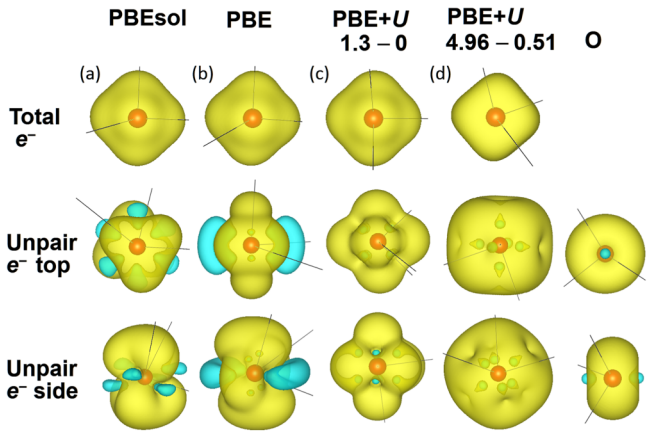

FIG. 17. e^- and unpaired e^- iso-density surface in the Ti atom calculated using (a) PBEsol, (b) PBE, (c) PBE + *U* [U_{eff}(Ti) = 1.3 eV], and (d) PBE + *U* [U_{eff}(Ti) = 4.45 eV]. The second and third rows show the top and side views of unpaired e^- iso-density surfaces, respectively. Yellow and blue colors represent the density of up- and down-spin, respectively. Orange spheres show the inner cores. The rightmost figures show unpaired e^- iso-density surfaces of the O atom, which is unchanged by U_{eff}(O).

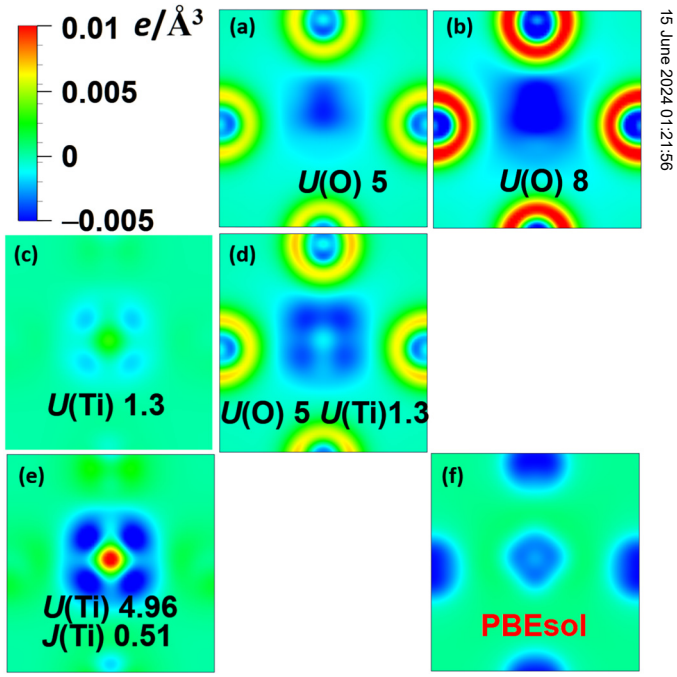

FIG. 18. Difference in e^- density *n* between PBE and PBE + *U* for typical *U* [(a)–(e)]; i.e., *n*(PBE + *U*) – *n*(PBE). (f) *n*(PBEsol) – *n*(PBE). The ion positions are the same for all results. Numbers are the values of *U* for O [*U*(O)] and Ti [*U*(Ti)] and *J* for Ti in eV. The *U* and *J* values that are not shown are zero.

densities. Both the e^- density and the unpaired e^- density became rounded or isotropic by U_{eff}(Ti), especially U_{eff}(Ti) = 4.45 eV, which explains the destruction of FE. In Fig. 17, the unpaired e^- density by PBEsol is less anisotropic than that by PBE. This explains the P_S, c/a, and FE-phase energy given by PBEsol that were smaller than those given by PBE.

Figure 18 shows the valence e^- density n in a BTO unit cell. U_{eff} (Ti) on Ti_{3d} orbit moves e^- of the anisotropic outer orbits into the Ti core region, implying the decrease of anisotropic n for the bonding with O and, hence, the decrease in the resistance against deformation. U_{eff} (O) on O_{2p} moves e^- of the less anisotropic inner orbits of O and Ti into the outer orbits of O, by which the anisotropy of n does not much decrease. Hence, U_{eff} (O) is expected to retain or increase the resistance against deformation and almost retain the anisotropy for FE.

REFERENCES

[1]M. E. Lines and A. M. Glass, *Principles and Applications of Ferroelectric and Related Materials* (Oxford University Press, Oxford, 1977).
[2]D. Ji *et al.*, "Freestanding crystalline oxide perovskites down to the monolayer limit," Nature **570**, 87 (2019).
[3]Y. Watanabe, D. Matsumoto, Y. Urakami, A. Masuda, S. Miyauchi, S. Kaku, S.-W. Cheong, and M. Yamato, see http://arxiv.org/abs/2210.12600 for "Free electrons holes and novel surface polar order in tetragonal $BaTiO_3$ ground states."
[4]D. I. Bilc, R. Orlando, R. Shaltaf, G.-M. Rignanese, J. Íñiguez, and P. Ghosez, "Hybrid exchange-correlation functional for accurate prediction of the electronic and structural properties of ferroelectric oxides," Phys. Rev. B **77**, 165107 (2008).
[5]R. Wahl, D. Vogtenhuber, and G. Kresse, "$SrTiO_3$ and $BaTiO_3$ revisited using the projector augmented wave method: Performance of hybrid and semilocal functionals," Phys. Rev. B **78**, 104116 (2008).
[6]Y. Watanabe, "Ferroelectricity of stress-free and strained pure $SrTiO_3$ revealed by *ab initio* calculations with hybrid and density functionals," Phys. Rev. B **99**, 064107 (2019).
[7]W. Kohn and L. J. Sham, "Self-consistent equations including exchange and correlation effects," Phys. Rev. **140**, A1133 (1965).
[8]J. P. Perdew, K. Burke, and M. Ernzerhof, "Generalized gradient approximation made simple," Phys. Rev. Lett. **77**, 3865–3868 (1996).
[9]J. P. Perdew, A. Ruzsinszky, G. I. Csonka, O. A. Vydrov, G. E. Scuseria, L. A. Constantin, X. Zhou, and K. Burke, "Restoring the density-gradient expansion for exchange in solids and surfaces," Phys. Rev. Lett. **100**, 136406 (2008).
[10]Z. Wu and R. E. Cohen, "More accurate generalized gradient approximation for solids," Phys. Rev. B **73**, 235116 (2006).
[11]J. Tao, J. P. Perdew, V. N. Staroverov, and G. E. Scuseria, "Climbing the density functional ladder: Nonempirical meta–generalized gradient approximation designed for molecules and solids," Phys. Rev. Lett. **91**, 146401 (2003).
[12]J. Sun, M. Marsman, G. I. Csonka, A. Ruzsinszky, P. Hao, Y.-S. Kim, G. Kresse, and J. P. Perdew, "Self-consistent meta-generalized gradient approximation within the projector-augmented-wave method," Phys. Rev. B **84**, 035117 (2011).
[13]A. Paul, J. Sun, J. P. Perdew, and U. V. Waghmare, "Accuracy of first-principles interatomic interactions and predictions of ferroelectric phase transitions in perovskite oxides: Energy functional and effective Hamiltonian," Phys. Rev. B **95**, 054111 (2017).
[14]L. Schimka, J. Harl, and G. Kresse, "Improved hybrid functional for solids: The HSEsol functional," J. Chem. Phys **134**, 024116 (2011).
[15]J. Heyd, G. E. Scuseria, and M. Ernzerhof, "Hybrid functionals based on a screened Coulomb potential," J. Chem. Phys. **118**, 8207 (2003).
[16]A. F. Devonshire, "Theory of barium titanate," Philos. Mag. Ser. 7 **40**, 1040 (1949).
[17]H. Uwe and T. Sakudo, "Stress-induced ferroelectricity and soft phonon modes in $SrTiO_3$," Phys. Rev. B **13**, 271–286 (1976).
[18]J. G. Bednorz and K. A. Müller, "$Sr_{1-x}Ca_xTiO_3$: An XY quantum ferroelectric with transition to randomness," Phys. Rev. Lett. **52**, 2289 (1984).
[19]N. Yanase, K. Abe, N. Fukushima, and T. Kawakubo, "Thickness dependence of ferroelectricity in heteroepitaxial $BaTiO_3$ thin film capacitors," Jpn. J. Appl. Phys. **38**, 5305 (1999).
[20]K. Abe, S. Komatsu, N. Yanase, K. Sano, and T. Kawakubo, "Asymmetric ferroelectricity and anomalous current conduction in heteroepitaxial $BaTiO_3$ thin films," Jpn. J. Appl. Phys. **36**, 5846 (1997).
[21]T. Schimizu and T. Kawakubo, "First-principles approach to the effect of c-axis elongation of $BaTiO_3$ thin films," Jpn. J. Appl. Phys. **37**, L235 (1998).
[22]H. Terauchi, Y. Watanabe, H. Kasatani, K. Kamigaki, Y. Yano, T. Terashima, and Y. Bando, "Structural study of epitaxial $BaTiO_3$ crystals," J. Phys. Soc. Jpn. **61**, 2194 (1992).
[23]Y. Watanabe, Y. Matsumoto, H. Kunitomo, M. Tanamura, and E. Nishimoto, "Crystallographic and electrical properties of epitaxial $BaTiO_3$ film grown on conductive and insulating perovskite oxides," Jpn. J. Appl. Phys. **33**, 5182 (1994).
[24]I. Kanno, S. Hayashi, M. Kitagawa, R. Takayama, and T. Hirao, "Antiferroelectric $PbZrO_3$ thin films prepared by multi-ion-beam sputtering," Appl. Phys. Lett **66**, 145 (1995).
[25]Y. Yano, K. Iijima, Y. Daitoh, T. Terashima, Y. Bando, Y. Watanabe, H. Kasatani, and H. Terauchi, "Epitaxial growth and dielectric properties of $BaTiO_3$ films on Pt electrodes by reactive evaporation," J. Appl. Phys. **76**, 7833 (1994).
[26]M. J. Haun, E. Furman, S. J. Jang, H. A. McKinstry, and L. E. Cross, "Hermodynamic theory of $PbTiO_3$," J. Appl. Phys. **62**, 3331 (1987).
[27]Y. L. Li, L. E. Cross, and L. Q. Chen, "A phenomenological thermodynamic potential for single crystals," J. Appl. Phys. **98**, 064101 (2005).
[28]Y. Watanabe, "Theoretical stability of the polarization in insulating-ferroelectric/ semiconductor structures," J. Appl. Phys. **83**, 2179–2193 (1998); Erratum: J. Appl. Phys. **84**, 3428 (1998).
[29]Y. Watanabe, "Theoretical stability of the polarization in a thin semiconducting ferroelectric," Phys. Rev. B **57**, 789 (1998).
[30]K. J. Choi *et al.*, "Enhancement of ferroelectricity in strained $BaTiO_3$ thin films," Science **306**, 1005 (2004).
[31]M. Tyunina, M. Savinov, and A. Dejneka, "Small-polaron conductivity in perovskite ferroelectric $BaTiO_3$ films," Appl. Phys. Lett. **121**, 202901 (2022).
[32]Y. G. Girshberg, E. V. Bursian, and Y. A. Grushevsky, "The mobility anisotropy in tetragonal $BaTiO_3$ in small polaron model," Ferroelectrics **6**, 53 (1973).
[33]Y. Watanabe, M. Okano, and A. Masuda, "Surface conduction on insulating $BaTiO_3$ crystal suggesting an intrinsic surface electron layer," Phys. Rev. Lett. **86**, 332 (2001).
[34]M. Choi, F. Oba, and I. Tanaka, "Electronic and structural properties of the oxygen vacancy in $BaTiO_3$," Appl. Phys. Lett. **98**, 172901 (2011).
[35]N. Tsunoda, Y. Kumagai, and F. Oba, "Stabilization of small polarons in $BaTiO_3$ by local distortions," Phys. Rev. Mater. **3**, 114602 (2019).
[36]A. Janotti, J. B. Varley, M. Choi, and C. G. Van de Walle, "Vacancies and small polarons in $SrTiO_3$," Phys. Rev. B **90**, 085202 (2014).
[37]M. Youssef, B. Yildiz, and K. J. Van Vliet, "Thermomechanical stabilization of electron small polarons in $SrTiO_3$ assessed by the quasiharmonic approximation," Phys. Rev. B **95**, 161110(R) (2017).
[38]F. Wang, W. Chu, L. Huber, T. Tu, Y. Dai, J. Wang, H. Peng, J. Zhao, and X.-Y. Zhu, "Phonon signatures for polaron formation in an anharmonic semiconductor," PNAS **119**, e2122436119 (2022).
[39]N. Ashcroft and N. D. Mermin, *Solid State Physics* (Saunders College Publishing, 1976). See www.cengage.com/c/solid-state-physics-1e-ashcroft/9780030839931/.
[40]H. Shigetani, K. Kobayashi, M. Fujimoto, W. Sugimura, Y. Matsui, and J. Tanaka, "$BaTiO_3$ thin films grown on $SrTiO_3$ substrates by a molecular-beam-epitaxy method using oxygen radicals," J. Appl. Phys. **81**, 693 (1997).
[41]A. Petraru, N. A. Pertsev, H. Kohlstedt, U. Poppe, R. Waser, A. Solbach, and U. Klemradt, "Polarization and lattice strains in epitaxial $BaTiO_3$ films grown by high-pressure sputtering," J. Appl. Phys. **101**, 114106 (2007).

[42]Y. Watanabe, "Calculation of strained $BaTiO_3$ with different exchange correlation functionals examined with criterion by Ginzburg-Landau theory, uncovering expressions by crystallographic parameters," J. Chem. Phys. **148**, 194702 (2018).
[43]A. I. Liechtenstein, V. I. Anisimov, and J. Zaanen, "Density-functional theory and strong interactions: Orbital ordering in Mott-Hubbard insulators," Phys. Rev. B **52**, R5467 (1995).
[44]S. L. Dudarev, G. A. Botton, S. Y. Savrasov, C. J. Humphreys, and A. P. Sutton, "Electron-energy-loss spectra and the structural stability of nickel oxide: An LSDA + U study," Phys. Rev. B **57**, 1505 (1998).
[45]M. E. Arroyo-de Dompablo, A. Morales-García, and M. Taravillo, "DFT + U calculations of crystal lattice, electronic stability under pressure of TiO_2 polymorphs," J. Chem. Phys. **135**, 054503 (2011).
[46]J. Muscat, V. Swamy, and N. M. Harrison, "First-principles calculations of the phase stability of TiO_2," Phys. Rev. B **65**, 224112 (2002).
[47]A. Fahmi, C. Minot, B. Silvi, and M. Causá, "Theoretical analysis of the structures of titanium dioxide crystals," Phys. Rev. B **47**, 11717 (1993).
[48]M. Cococcioni and S. de Gironcoli, "Linear response approach to the calculation of the effective interaction parameters in the LDA + U method," Phys. Rev. B **71**, 035105 (2005).
[49]Z. Hou and K. Terakura, "Defect states induced by oxygen vacancies in cubic $SrTiO_3$: First-principles calculations," J. Phys. Soc. Jpn. **79**, 114704 (2010).
[50]N. A. Deskins and M. Dupuis, "Electron transport via polaron hopping in bulk TiO_2: A density functional theory characterization," Phys. Rev. B **75**, 195212 (2007).
[51]X. Hao, Z. Wang, M. Schmid, U. Diebold, and C. Franchini, "Coexistence of trapped and free excess electrons in $SrTiO_3$," Phys. Rev. B **91**, 085204 (2015).
[52]G. Gebreyesus, L. Bastonero, M. Kotiuga, N. Marzari, and I. Timrov, "Understanding the role of Hubbard corrections in the rhombohedral phase of $BaTiO_3$," Phys. Rev. B **108**, 235171 (2023).
[53]N. A. Deskins and M. Dupuis, "Intrinsic hole migration rates in TiO_2 from density functional theory," J. Phys. Chem. C **113**, 346 (2009).
[54]P. Erhart, A. Klein, D. Åberg, and B. Sadigh, "Efficacy of the DFT + *U* formalism for modeling hole polarons in perovskite oxides," Phys. Rev. B **90**, 035204 (2014).
[55]T. Nakatani, A. Yoshiasa, A. Nakatsuka, T. Hiratoko, T. Mashimo, M. Okube, and S. Sasaki, "Variable-temperature single-crystal x-ray diffraction study of tetragonal and cubic perovskite-type barium titanate," Acta Cryst. **72**, 151 (2016).
[56]H. H. Wieder, "Electrical behavior of barium titanate single crystals at low temperatures," Phys. Rev. **99**, 1161–1165 (1955).
[57]S. H. Wemple, M. Didomenico, Jr., and I. Camlibel, "Dielectric and optical properties of melt-grown $BaTiO_3$," J. Phys. Chem. Solids **29**, 1797 (1968).
[58]A. Okazaki and M. Kawaminami, "Lattice constant of strontium titanate at low temperatures," Mat. Res. Bull. **8**, 545 (1973).
[59]R. Loetzsch, A. Lübcke, I. Uschmann, E. Förster, V. Große, M. Thuerk, T. Koettig, F. Schmidl, and P. Seidel, "The cubic to tetragonal phase transition in single crystals near its surface under internal and external strains," Appl. Phys. Lett. **96**, 071901 (2010).
[60]Y. Luspin, J. L. Servoin, and F. Gervais, "Soft mode spectroscopy in barium titanate," J. Phys. C **13**, 3761 (1980).
[61]A. Scalabrin, A. S. Chaves, D. S. Shim, and S. P. S. Porto, "Temperature dependence of the A1 and E optical phonons in $BaTiO_3$," Phys. Status Solidi B **79**, 731 (1977).
[62]W. G. Stirling, "Neutron inelastic scattering study of the lattice dynamics of strontium titanate: Harmonic models," J. Phys. C: Solid State Phys. **5**, 2711 (1972).
[63]W. G. Spitzer, R. C. Miller, D. A. Kleinman, and L. E. Howarth, "Far infrared dielectric dispersion in $BaTiO_3$, $SrTiO_3$, and TiO_2," Phys. Rev. **126**, 1710 (1962).
[64]H. Vogt and G. Neumann, "Observation of infrared active and silent modes in cubic crystals by hyper-Raman scattering," Phys. Status Solidi B **92**, 57 (1979).
[65]H. Unoki and T. Sakudo, "Electron spin resonance of Fe^{3+} in $SrTiO_3$ with special reference to the 110 K phase transition," J. Phys. Soc. Jpn. **23**, 546 (1967).
[66]K. A. Müller and W. Berlinger, "Static critical exponents at structural phase transitions," Phys. Rev. Lett. **26**, 13 (1971).
[67]M. Springer and F. Aryasetiawan, "Frequency-dependent screened interaction in Ni within the random-phase approximation," Phys. Rev. B **57**, 4364 (1998).
[68]I. Solovyev, N. Hamada, and K. Terakura, "T_{2g} versus all 3d localization in $LaMO_3$ perovskites (Ti–Cu): First-principles study," Phys. Rev. B **53**, 176403 (1996).
[69]E. Pavarini, S. Biermann, A. Poteryaev, A. I. Lichtenstein, A. Georges, and O. K. Andersen, "Mott transition and suppression of orbital fluctuations in orthorhombic $3d^1$ perovskites," Phys. Rev. Lett. **92**, 176403 (2004).
[70]C. Persson and A. F. da Silva, "Strong polaronic effects on rutile TiO_2 electronic band edges," Appl. Phys. Lett. **86**, 231912 (2005).
[71]Z. Hu and H. Metiu, "Choice of U for DFT + U calculations for titanium oxides," J. Phys. Chem. C **115**, 5841 (2011).
[72]P. E. Blöchl, "Projector augmented-wave method," Phys. Rev. B **50**, 17953–17979 (1994).
[73]P. Blaha, K. Schwarz, G. K. H. Madsen, D. Kvasnicka, J. Luitz, R. Laskowski, F. Tran, and L. D. Marks, see http://www.wien2k.at/reg_user/textbooks/usersguide.pdf for "User's guide, WIEN2k" (2023).
[74]Y. Watanabe, "Examination of permittivity for depolarization field of ferroelectric by *ab initio* calculation, suggesting hidden mechanisms," Sci. Rep. **11**, 2155 (2021).
[75]G. Kresse and J. Hafner, "*Ab initio* molecular dynamics for liquid metals," Phys. Rev. B **47**, 558R (1993).
[76]G. Kresse and J. Furthmüller, "Efficiency of ab-initio total energy calculations for metals and semiconductors using a plane-wave basis set," Comput. Mater. Sci. **6**, 15–50 (1996).
[77]G. Kresse and D. Joubert, "From ultrasoft pseudopotentials to the projector augmented-wave method," Phys. Rev. B **59**, 1758 (1999).
[78]R. Resta, "Theory of the electric polarization in crystals," Ferroelectrtics **136**, 51 (1992).
[79]H. J. Monkhorst and J. D. Pack, "Special points for Brillouin-zone integrations," Phys. Rev. B **13**, 5188–5192 (1976).
[80]Y. Watanabe, "Accurate semiempirical analytical formulas for spontaneous polarization by crystallographic parameters of $SrTiO_3$-$BaTiO_3$ system by *ab initio* calculations," Comput. Mater. Sci. **158**, 315–323 (2019).
[81]G. Makov and M. C. Payne, "Periodic boundary conditions in *ab initio* calculations," Phys. Rev. B **51**, 4014 (1996).
[82]M. Hacene, A. A. Sedrakian, X. Rozanska, D. Klahr, T. Guignon, and P. F. Lessard, "Accelerating VASP electronic structure calculations using graphic processing units," J. Comput. Chem. **33**, 2581 (2012).
[83]M. Hutchinson and M. Widom, "VASP on a GPU: Application to exact-exchange calculations of the stability of elemental boron," Comput. Phys. Commun. **7**, 1422 (2011).
[84]K. Momma and F. Izumi, "VESTA 3 for three-dimensional visualization of crystal, volumetric and morphology data," J. Appl. Crystallogr. **44**, 1272 (2011).
[85]A. W. Hewat, "Structure of rhombohedral ferroelectric barium titanate," Ferroelectrics **6**, 215 (1973).
[86]H. F. Kay and P. Vousden, "Symmetry changes in barium titanate at low temperatures and their relation to its ferroelectric properties," Philos. Mag. Ser. 7 **40**, 1019 (1949).
[87]K. A. Müller and H. Burkard, "$SrTiO_3$: An intrinsic quantum paraelectric below 4 K," Phys. Rev. B **19**, 3593 (1979).
[88]H. E. Weaver, "Dielectric properties of single crystals of $SrTiO_3$ at low temperatures," J. Phys. Chem. Solids **11**, 274 (1959).
[89]R. Wördenweber, E. Hollmann, R. Kutzner, and J. Schubert, "Induced ferroelectricity in strained epitaxial $SrTiO_3$ films on various substrates," J. Appl. Phys. **102**, 044119 (2007).
[90]R. O. Bell and G. Rupprecht, "Elastic constants of strontium titanate," Phys. Rev. **129**, 90 (1963).
[91]S. Körbel, J. Hlinka, and S. Sanvito, "Electron trapping by neutral pristine ferroelectric domain walls in $BiFeO_3$," Phys. Rev. B **98**, 100104(R) (2018).
[92]H. A. A. Khan, S. Ullah, G. Rehman, S. Khan, and I. Ahmad, "First principle study of band gap nature, spontaneous polarization, hyperfine field and electric

field gradient of desirable multiferroic bismuth ferrite ($BiFeO_3$)," J. Phys. Chem. Solids **148**, 109737 (2021).
[93]R. I. Eglitis and R. Jia, "Review of systematic tendencies in (001), (011) and (111) surfaces using B3PW as well as B3LYP computations of $BaTiO_3$, $CaTiO_3$, $PbTiO_3$, $SrTiO_3$, $BaZrO_3$, $CaZrO_3$, $PbZrO_3$ and $SrZrO_3$ perovskites," Materials **16**, 7623 (2023).
[94]R. I. Eglitis and A. I. Popov, "Systematic trends in (001) surface *ab initio* calculations of ABO_3 perovskites," J. Saudi Chem. Soc. **22**, 459–468 (2018).
[95]K. Dayal and K. Bhattacharya, "A real-space non-local phase-field model of ferroelectric domain patterns in complex geometries," Acta Mater. **55**, 1907 (2007).